Nanoscale

PAPER

Controlling photoinduced electron transfer from PbS@CdS core@shell quantum dots to metal oxide nanostructured thin films†

Cite this: *Nanoscale*, 2014, **6**, 7004

H. Zhao,[ab] Z. Fan,[c] H. Liang,[b] G. S. Selopal,[ad] B. A. Gonfa,[b] L. Jin,[b] A. Soudi,[b] D. Cui,[b] F. Enrichi,[e] M. M. Natile,[fg] I. Concina,[ad] D. Ma,[b] A. O. Govorov,*[c] F. Rosei*[bh] and A. Vomiero*[ab]

Received 21st March 2014
Accepted 22nd April 2014

DOI: 10.1039/c4nr01562b

www.rsc.org/nanoscale

N-type metal oxide solar cells sensitized by infrared absorbing PbS quantum dots (QDs) represent a promising alternative to traditional photovoltaic devices. However, colloidal PbS QDs capped with pure organic ligand shells suffer from surface oxidation that affects the long term stability of the cells. Application of a passivating CdS shell guarantees the increased long term stability of PbS QDs, but can negatively affect photoinduced charge transfer from the QD to the oxide and the resulting photoconversion efficiency (PCE). For this reason, the characterization of electron injection rates in these systems is very important, yet has never been reported. Here we investigate the photoelectron transfer rate from PbS@CdS core@shell QDs to wide bandgap semiconducting mesoporous films using photoluminescence (PL) lifetime spectroscopy. The different electron affinity of the oxides (SiO_2, TiO_2 and SnO_2), the core size and the shell thickness allow us to fine tune the electron injection rate by determining the width and height of the energy barrier for tunneling from the core to the oxide. Theoretical modeling using the semi-classical approximation provides an estimate for the escape time of an electron from the QD 1S state, in good agreement with experiments. The results demonstrate the possibility of obtaining fast charge injection in near infrared (NIR) QDs stabilized by an external shell (injection rates in the range of 110–250 ns for TiO_2 films and in the range of 100–170 ns for SnO_2 films for PbS cores with diameters in the 3–4.2 nm range and shell thickness around 0.3 nm), with the aim of providing viable solutions to the stability issues typical of NIR QDs capped with pure organic ligand shells.

1. Introduction

Colloidal quantum dots (QDs) have been recently employed in several technologically relevant applications such as photodetectors,[1] light emitting technologies[2–4] and excitonic (third generation) solar cells.[5,6] In the latter case, they paved the way for the development of low cost solar cells fabricated through low temperature processes.[2] The photoconversion efficiency (PCE) was boosted up to 7% in solar cells based on QDs, by using nanocrystals able to absorb near infrared (NIR) radiation.[7] For these reasons, QDs represent a concrete pathway for a significant breakthrough in the field. However, a major drawback of QDs is their limited stability under standard processing or operation conditions, since they are sensitive to the surface chemical environment (ligand variation, surface oxidation, surface etching, *etc.*), moisture, oxygen, temperature and/or light.[8] Such sensitivity could lead to the presence of surface defects that act as charge traps, leading to a decrease of PCE.[8] A promising solution to address this challenge consists in using core@shell structured QDs, which have shown significantly enhanced quantum yield (QY) and largely improved chemical, thermal and photochemical stability with respect to the pure QDs capped with organic ligands only.[9–12] Recently, attracted by their excellent properties, core@shell QDs have been explored as potential light absorbers in solar cells.[10–12]

In most solar cell architectures based on QDs as light harvesters, anodic charge transport is carried out by a wide

[a]*CNR-INO SENSOR Lab, Via Branze 45, 25123 Brescia, Italy. E-mail: alberto.vomiero@ing.unibs.it*

[b]*Institut National de la Recherche Scientifique, 1650 Boulevard Lionel-Boulet, Varennes, Québec J3X 1S2, Canada. E-mail: rosei@emt.inrs.ca*

[c]*Physics and Astronomy Department, Ohio University, Athens, Ohio 45701, USA. E-mail: govorov@helios.phy.ohiou.edu*

[d]*SENSOR Lab Department of Information Engineering, University of Brescia, Via Valotti 9, 25133 Brescia, Italy*

[e]*Laboratorio Nanofab-Veneto Nanotech, Via delle Industrie 5, 30175 Marghera, Italy*

[f]*CNR-IENI, via F. Marzolo 1, 35131 Padova, Italy*

[g]*Department of Chemical Science, University of Padova, via F. Marzolo 1, 35131 Padova, Italy*

[h]*Center for Self-Assembled Chemical Structures, McGill University, H3A 2K6 Montreal, Quebec, Canada*

† Electronic supplementary information (ESI) available: TEM image of silica particle, photos of QDs/oxide composite, the lifetime of QDs/oxide composite with the PbS core size of 4.8 nm and the absorption and PL spectra of QDs or QDs/oxide composite. See DOI: 10.1039/c4nr01562b

band gap oxide semiconductor.[13] Electrons are injected from QDs to the oxide, generating the photocurrent. This is why one of the most important issues for improving device efficiency is to understand and control the fast exciton dissociation at the QD/oxide interface, and charge injection into the anodic material. Depending on the relative alignment of conduction- and valence-band edges of the core and shell, core@shell QDs can be classified as type-I (both the electrons and holes are confined in the core region),[9,14] type-II (electrons and holes are spatially separated into core and shell regions)[15,16] and quasi type-II, in which one type of charge carrier is delocalized over the entire core@shell structure, while the other type is localized in the core or shell region.[11,17] Besides the efficient electron extraction from type-II ZnSe@CdS core@shell QDs[12] and quasi-type-II PbSe@PbS QDs,[11] Dworak *et al.* demonstrated electron extraction from the photoexcited core in type-I visible-emitting CdSe@CdS QDs by using the molecular scavenger,[10] in which the electron transfer rate strongly depends on the CdS shell thickness. Although the synthesis of NIR core@shell QDs, such as PbS@CdS, PbSe@CdSe and InP@ZnS, has been recently reported,[18–21] investigations on their charge transfer into electron scavengers, which are essential for designing and achieving optimal NIR-responsive solar cells, are still very limited[11,17,22] and no investigation is reported on charge transfer from QD to an oxide scaffold, which is the natural host of QDs for QD solar cells. The mechanism of charge transfer in these NIR core@shell QDs after combination with nanoscale wide bandgap metal oxides (which are typically used as electron transporting media) is still unclear:[8,11] while QDs absorbing in the visible range (like the aforementioned CdS, CdSe and core–shell counterparts) present favorable band alignment for electron injection from QDs to TiO_2, irrespective of their size, the position of 1S state NIR absorbing PbS QDs varies significantly with QD size, and a threshold size exists, above which electron transfer to TiO_2 is energetically unfavorable.[23]

Here, we report a systematic investigation of the photoexcited electron transfer from the NIR core@shell PbS@CdS QDs to metal oxide nanostructured thin films (SiO_2, TiO_2 or SnO_2, see Scheme 1). The core@shell QDs were loaded into the mesoporous film using a bifunctional linker molecule (mercaptoacetic acid, MAA). We observe that the electron transfer rate is strongly dependent on PbS core size, CdS shell thickness and the type of oxide. To understand our findings, we modeled the tunneling process using the quasi-classical approximation. This allowed us to describe the trends observed in the experiments. Due to the much higher stability of the core@shell QDs as compared to standard PbS QDs, our findings suggest that the PbS@CdS QDs can be effectively used for the development of highly efficient and stable light absorbers in PV devices.[24]

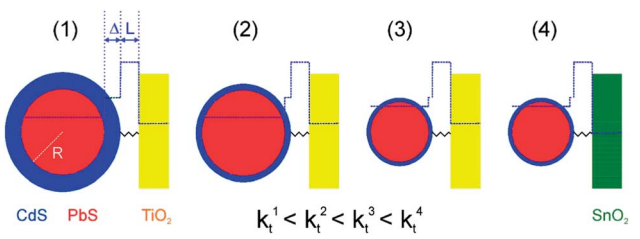

Scheme 1 Scheme of the PbS@CdS core@shell QDs bound to TiO_2 or SnO_2 surface through mercaptoacetic acid (MAA) ligand. The position of electronic conduction bands is sketched (not to scale) as a function of core size, shell thickness and QD–oxide distance. Electron injection rate k_t is supposed to increase from 1 to 4, as confirmed by experimental findings and theoretical calculations.

2. Experimental

2.1 Materials

Lead chloride (98%), sulfur (100%), oleylamine (OLA) lead acetate trihydrate, trioctylphosphine (TOP 90%), bis-(trimethylsilyl) sulfide $(TMS)_2S$, (technical grade, 70%), cadmium oxide (99%), oleic acid (OA), MAA, 1-octadecene (ODE), tetraethyl orthosilicate (TEOS), acetonitrile, ammonium hydroxide (29%), $SnCl_4$, and hydrochloric acid were obtained from Sigma-Aldrich Inc. Hexane, toluene, and ethanol were purchased from Fisher Scientific Company. TiO_2 paste composed of 20 nm sized anatase nanoparticles was purchased from Dyesol (18 NR-T). SnO_2 paste was prepared by mixing a proper amount of SnO_2 nanoparticles (about 1 g) with ethyl-cellulose (0.5 g) and α-terpineol (Sigma-Aldrich) (1 mL), using water–ethanol (5/1 v/v) as a dispersion medium. All chemicals were used as purchased.

2.2 Synthesis

2.2.1 Synthesis of PbS QDs. PbS QDs were synthesized by using OLA as ligand.[12] Typically, $PbCl_2$ (3.6 mmol) in OLA (2.4 mL) and sulfur (0.36 mmol) in OLA (0.24 mL) were purged, respectively, by N_2 at room temperature for 30 min. The $PbCl_2$–OLA suspension was heated to 160 °C and kept at this temperature for 1 hour. The $PbCl_2$–OLA suspension was cooled to 120 °C under vacuum for 15 min. The flask was then reopened and the N_2 flux was restored. Sulfur in OLA at room temperature was quickly injected into the $PbCl_2$–OLA suspension under vigorous stirring. The reaction cell was quenched with cold water after the growth reaction was conducted at 100 °C for 1–360 min. The size of PbS QDs can be modulated from 3.4 nm to 6 nm by adjusting the molar ratio of Pb/S, injection temperature and growth time.[12] For purification, ethanol was added, then the suspension was centrifuged and the supernatant was removed. The pure PbS QDs capped with OLA were then re-dispersed in OA–toluene (v/v 1/20). After precipitation with ethanol and centrifugation, the QDs are re-dispersed in toluene and the exchange is repeated twice. Finally, the QDs were dispersed in toluene.

PbS QDs with diameter of 3.0 nm were synthesized by using OA as ligands.[25] In a typical synthesis, a mixture of lead acetate trihydrate (1 mmol), OA (1.2 mL), TOP (1 mL), and ODE (15 mL) were heated to 150 °C for 1 h. Then, the system was cooled to ~100 °C under vacuum for 15 min. Subsequently, the solution containing 0.5 mmol $(TMS)_2S$, 0.2 mL of TOP and 4.8 mL of ODE was quickly injected into the reaction flask at 130 °C; then, the reaction was quenched by immersing the reaction flask into cold water. PbS QDs were precipitated with ethanol, centrifuged

to remove unreacted lead oleate and free OA molecules and then re-dispersed in toluene.

2.2.2 Synthesis of PbS@CdS QDs. PbS@CdS QDs with a thin shell were synthesized *via* a cation exchange method.[10] Typically, CdO (2.3 mmol), OA (2 mL) and ODE (10 mL) were heated to 255 °C under N_2 for 20 min. The clear solution was cooled to 155 °C under vacuum for 15 min. The flask was then reopened and the N_2 flux was restored. PbS QDs suspension in toluene (1 mL, absorbance = 3 at the first exciton peak) was diluted in 10 mL toluene, bubbled for 30 min and then heated to 100 °C immediately. The Cd–OA mixture was injected. The reaction cell was quenched with cold water after the growth reaction was conducted at 100 °C for different time. PbS@CdS QDs with tunable core sizes and constant shell thickness of 0.7 nm was synthesized by choosing different starting PbS sizes together with different reaction parameters (Pb-to-Cd ratio and reaction time).

2.2.3 Synthesis of SiO_2 particles. The silica particles were synthesized *via* the Stöber approach.[26] Typically, 1 mL of ammonium hydroxide was mixed with 1.1 mL of water and 7.4 mL of alcohol. Then the mixture was stirred at 600 rpm for 10 minutes. Subsequently, 0.56 mL of TEOS was added to the above mixture: the mixture was then stirred for 72 hours at room temperature. The particles were centrifuged and re-dispersed in alcohol. This process was repeated three time and the particles were dried at 80 °C for 12 hours.

2.2.4 Synthesis of SnO_2 particles. In a three necks flask 1.2 mL $SnCl_4$ were added to 100 mL methanol. Once the HCl fumes had disappeared, 4 mL NH_3 (30%) were added dropwise to the reaction mixture, which was left to react for about 10–15 minutes. The raw product was then dried at 80 °C overnight for solvent removal, then SnO_2 was obtained by calcinating at 450 °C for 2 h under air atmosphere.

2.3 Functionalization of oxides and their subsequent hybridization with QDs

Mesoporous TiO_2 (SnO_2 or SiO_2) films were prepared by tape casting oxide paste onto transparent glass substrates.[27] The drying process was followed for 15 min at ambient atmosphere and temperature and then for 5 min at 110 °C. After drying, all the samples were then annealed at 450 °C for 30 min in ambient atmosphere. The thickness of the film was ~5 μm. MAA was used as a bifunctional linker to assist in adsorbing QDs on oxide.[28] Typically, the TiO_2 glass slides were introduced in a solution consisting of hydrochloric acid and deionized water for 20 min (pH 2). The slides were rinsed with deionized water and anhydrous acetonitrile, respectively and dried with nitrogen. Then the film was rinsed with anhydrous acetonitrile and incubated in a solution containing 1 M MAA and acetonitrile for 12 h. According to the literature,[28] MAA substitutes the long ligands (OA in the present study) at the contact point between QD and oxide. Accordingly, the distance between the QD and the oxide can be estimated as the length of MAA (0.61 nm). This distance is taken into account for the theoretical calculations of the electron injection rate. The films were subsequently washed with anhydrous acetonitrile and anhydrous toluene and placed directly in the QD toluene solution (1 μM) for 72 hours at −10 °C. Finally the film was thoroughly rinsed with toluene thoroughly and dried under nitrogen for further optical characterization.

2.4 Structural and optical characterization

The morphology of PbS@CdS QDs was determined using a JEOL 2100F transmission electron microscopy (TEM). For the core@shell QDs, the solution was directly drop casted on the Cu grid. For the observation of the QDs grafted on TiO_2 surface, the TiO_2 film was sonicated for 10 min into a toluene solution. Then the detached film formed a concentrated mixture that was drop casted on the Cu grid for TEM observation.

Absorption spectra were acquired with a Cary 5000 UV-visible-NIR spectrophotometer (Varian) with a scan speed of 600 nm min^{-1}. Fluorescence spectra were taken with a Fluorolog®-3 system (Horiba Jobin Yvon). The photoluminescence (PL) lifetime of QDs/oxide composite was measured using a pulsed laser diode of 444 nm and the multichannel scaling mode (MCS) by fixing the detection emission wavelength in different samples at the maximum of the size-dependent PL peak.

3. Results and discussion

3.1 Synthesis and structure of PbS@CdS core@shell QDs

Colloidal PbS QDs of various sizes in the range 3–6 nm were firstly synthesized and subsequently used to synthesize PbS@CdS QDs *via* the cation exchange approach.[20] As-synthesized PbS and

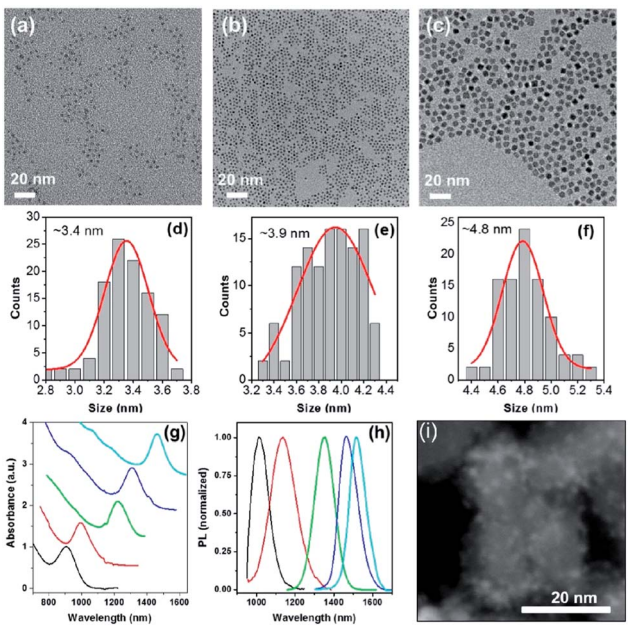

Fig. 1 Representative TEM images (a)–(c) and size distribution (d)–(f) of PbS@CdS QDs with average diameter of (a) and (d) ~3.4 ± 0.3 nm, (b) and (e) ~3.9 ± 0.3 nm and (c) and (f) ~4.8 ± 0.3 nm. Representative absorption (g) and emission (h) spectra of PbS@CdS QDs in solution. The same color indicates spectra from the same sample. (i) Representative TEM image of PbS@CdS QDs with ~3.0 nm core diameter (shell thickness ~0.2 nm) after anchoring to TiO_2 nanoparticles.

Table 1 Overall size of PbS@CdS QDs based on TEM observations, estimated core size and shell thickness from methods #1, first exciton absorption maxima, PL maxima in toluene. Method #1: core size estimated from absorption peak positions and shell thickness calculated by: overall size – core size

Entry	d_{total}	d_{core}	d_{shell}	Abs. max (nm)	PL max (nm)
1	6.0 ± 0.2	5.5	0.25	1464	1517
2	5.4 ± 0.2	4.8	0.3	1310	1465
3	4.8 ± 0.3	4.2	0.3	1221	1350
4	3.9 ± 0.3	3.4	0.25	994	1135
5	3.4 ± 0.3	3.0	0.2	905	1013
6	4.2 ± 0.3	3.0	0.6	895	1090
7	4.8 ± 0.3	3.4	0.7	1000	1160

PbS@CdS QDs exhibit a uniform size distribution (Fig. 1a–f). As previously reported, the shell of PbS@CdS QDs is mainly composed of CdS.[20,21] The average overall diameter of the pure PbS QDs or the core@shell QDs was estimated from TEM images. As-synthesized PbS and core@shell QDs exhibit a very well defined first-exciton absorption peak and PL peak. The absorption and PL spectra of selected samples with various sizes of PbS@CdS QDs in solution are shown in Fig. 1g and h. The core size was estimated from the exciton absorption peak.[21]

The overall QD diameter (d_{total}), core diameter (d_{core}), CdS shell thickness (d_{shell}), the maximum absorbance and PL peaks are listed in Table 1. The pure PbS and core@shell PbS@CdS QDs range from 3 nm to 6 nm with a typical QY of 19–85% in toluene, a <9% size distribution and a lifetime of 1–3 μs, indicating that our synthesis yields good quality QDs, consistent with the PbS QDs reported in the literature.[20,21] In fact, even with very thin shell, around 0.1–0.3 nm, the QY and stability of plain PbS QDs can be largely enhanced.[20,24]

The electron transfer behavior of PbS@CdS QDs was investigated by loading QDs on mesoporous thin films prepared by standard tape casting oxide paste onto transparent glass substrates. The films were composed of wide bandgap nanoparticles (TiO_2 and SnO_2 were used) attached to the QDs *via* MAA linker, the thiol groups binding to the QDs surface and the carboxylic groups binding to the oxide surface.[23,29] The QDs/oxide film appears brown due to the presence of the QDs (Fig. S1†). Silica nanoparticle (SiO_2) films (Fig. S2†) were used as benchmark, because the photoexcited electrons are not injected into the oxide in this case.[28] In all the experiments the same linker (MAA) was used to link the QDs and the oxide surface. As shown in Fig. 1i, the core@shell PbS@CdS QDs can be assembled onto the TiO_2 nanoparticles with very good dispersion without any aggregation.

3.2 Charge transfer *versus* energy transfer

Electron transfer between QDs and oxide was monitored through transient PL spectroscopy using a pulsed laser diode (excitation wavelength λ_{ex} = 444 nm) and a MCS set-up. The latter are widely used to probe the charge transfer process in QDs/electron scavenger systems (*e.g.* PbS/TiO_2, PbS/SnO_2, PbSe@CdSe/methylviologen and CdSe@CdS/methylviologen).[10,17,23,29,30] In general, lifetime variation can be ascribed to both energy and electron transfer processes between the QDs and the oxide.[23,29,31,32] For this reason, the experimental parameters should be carefully planned to discriminate between energy and charge transfer. Energy transfer may occur from QD to QD, from QD to oxide, or from QD to linker molecules. As mentioned above, in the present case the QDs are bound to the oxide surface through MAA. They are very well dispersed (Fig. 1i) and do not agglomerate, which rules out almost completely the possibility of QD–QD energy transfer. In addition, the MAA itself is reported not to quench the PL of QDs or to induce variation in lifetime.[23] As shown in Fig. S3a,† the absorption edge of MAA falls at around 300 nm. Thus absorption from MAA and PL emission from QD do not overlap, excluding any possible energy transfer between the QDs and the MAA ligand. Furthermore, the peak position and intensity in the PL spectra of QDs before and after addition of MAA do not show any significant change (Fig. S3b†), indicating that MAA does not quench QDs either by energy transfer or by change transfer, and allowing us to conclude that, also in the present case, MAA does not act as hole scavenger for PbS QDs.

To rule out the possibility of energy transfer from the QDs to oxide films, we measured the absorption and PL spectra of the QDs/TiO_2 system. TiO_2 films exhibit negligible absorbance in the spectral range 500 to 1200 nm (a), suggesting that energy transfer between QD and TiO_2 is a highly unfavorable process. The lowest exciton absorption peak of the core@shell QD in TiO_2 mesoporous film red-shifts by ~40 nm with respect to that of the pure core@shell QDs in solution (Fig. 2a) for a very thin shell (0.2 nm, equal to one monolayer of CdS). The emission peak of the core@shell QD–TiO_2 composite also red-shifts by about ~50 nm compared to the pure core@shell QDs in solution (Fig. 2b) for the same shell thickness, which is close to the spectral shift of the absorption peak. A similar phenomenon was also observed for the shell-free or core@shell QDs after combination with SnO_2 or SiO_2. This result is consistent with previously reported work on pure PbS QD/TiO_2, confirming that the red-shift is due to redistribution of electronic density and reduction of electron confinement. Other possible reasons may be the variation of refractive index surrounding the QDs and not to energy transfer processes.[29] We therefore attribute the

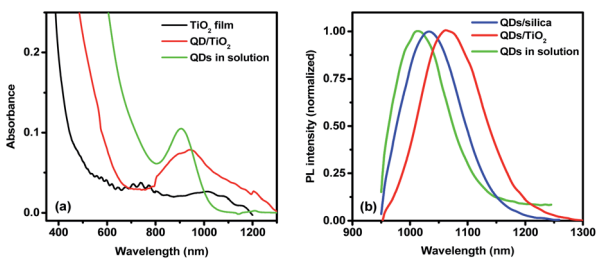

Fig. 2 (a) Representative absorption spectra of PbS@CdS QDs in solution and after uptake by TiO_2 film. The black line indicates the absorption spectrum of TiO_2 film. (b) Representative PL spectra of PbS@CdS QDs in solution and after uptake on SiO_2 and TiO_2 film. The PbS/CdS QDs have a core size of 3.0 nm and shell thickness of 0.2 nm.

variation of lifetime in QDs/TiO_2 and QDs/SnO_2 with respect to QDs/SiO_2 to the photo-excited charge transfer.

3.3 Electron transfer: the effect of oxide

According to Scheme 1, we investigated the electron transfer from PbS@CdS core@shell QDs with different core sizes (in the range 3.0–6.0 nm) and shell thickness (in the range 0–0.6 nm) to different oxides.[20] Pure PbS QDs with size in the range 3.0 to 5.2 nm were considered as a benchmark, to evaluate the effect of the shell on the charge injection rate. In core@shell systems we expect the shell to act as a barrier to be overcome through tunneling for the injection to take place. The PbS@CdS QDs with shell thickness of 0.2–0.3 nm show narrow core size distribution and uniform shell thickness.[22] The fluorescence decay for QDs attached on the oxide surface is reported in Fig. 3a and b for core diameter of 3.0 nm and 4.2 nm, respectively and constant shell thickness around 0.2–0.3 nm. The representative decay curves of the PL peak centered at ~1.18 eV (1050 nm) of PbS@CdS QDs were well fitted by a two-component decay, τ_1 and τ_2 being the short and long PL lifetime, respectively. The intensity-weighted average lifetime $\langle\tau\rangle$ is estimated using eqn (1) as follows:[32]

$$\langle\tau\rangle = \frac{a_1\tau_1{}^2 + a_2\tau_2{}^2}{a_1\tau_1 + a_2\tau_2} \quad (1)$$

where a_i ($i = 1,2$) are the coefficients of the fitting of PL decay.

The average PL lifetime of the core–shell (core size: 3.0 nm; shell: 0.2 nm) decreases from around (690 ± 5) ns in QDs/SiO_2 to (110 ± 5) ns in QDs/TiO_2, and further to (100 ± 5) ns in QDs/SnO_2. A similar trend was also observed for a core size of 4.2 nm and shell thickness of 0.3 nm (roughly corresponding to 1.5 monolayers coverage, Fig. 3b), indicating efficient electron transfer from the core@shell PbS@CdS QDs into both TiO_2 and SnO_2. The lifetime $\langle\tau\rangle$ scales according to the position of the conduction band (CB) of the oxide, the faster PL decrease occurring in SnO_2, as expected, since the electron affinity for TiO_2 is around −4.2 eV and that for SnO_2 is around −4.5 eV.[33] Then the driving force (ΔG^0) (the energy difference between the 1S state and the electron affinity for metal oxide) for the electron injection from the core@shell QDs to SnO_2 is 0.3 eV higher than that from QDs to TiO_2, which explains the faster injection. A similar trend was observed by Kamat and co-workers for CdSe QDs (without any protective shell) linked to SnO_2, ZnO and TiO_2.[34]

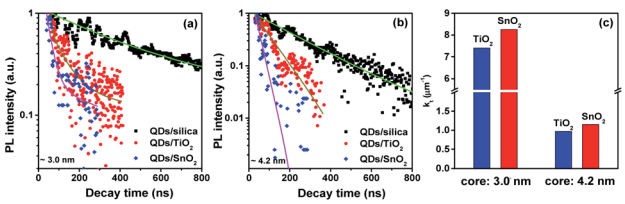

Fig. 3 Fluorescence decays of PbS@CdS QDs grafted on silica, TiO_2 and SnO_2 for different PbS core diameter: (a) 3.0 nm and (b) 4.2 nm. The shell thickness is approximately 0.2–0.3 nm. The excitation wavelength is λ_{ex} = 444 nm. All measurements were carried out at ambient temperature. (c) k_t for different oxides.

3.4 Electron transfer: the effect of core size

As mentioned previously, the decrease in lifetime is mainly attributed to electron transfer rather than energy transfer. Thus, the observed decrease of lifetime is a consequence of the photoexcited electron transfer from the PbS core to TiO_2 or SnO_2. The electron-transfer rate constant (k_t) was then estimated using the following equation, to provide a quantitative description of charge injection:[35]

$$k_t = \frac{1}{\langle\tau\rangle} - \frac{1}{\langle\tau\rangle_{SiO_2}} \quad (2)$$

where $\langle\tau\rangle$ and $\langle\tau\rangle_{SiO_2}$ are the average PL lifetimes of the QDs/TiO_2 (or QDs/SnO_2) and QDs/SiO_2, respectively. With the increase of PbS size, k_t decreased down to 0 (Fig. 3c, 4 and 5), indicating that no electron injection is possible beyond a certain threshold size, due to unfavorable electronic band alignment between QDs and oxide (see Scheme 1 and Fig. 5). For shell-free QDs, k_t with core size of 3.0 nm is as high as 11.3 ± 0.9 μs^{-1}, consistently with the value reported for PbS/TiO_2,[23] while the threshold size for injection is 5.2 nm. For shell thickness of 0.3 nm, k_t with core size of 3.0 nm is as high as 7.4 ± 0.3 μs^{-1}, while the threshold size is 4.8 nm (Fig. 4), possibly due to the charge injection barrier induced by the presence of the shell.[29] Hyun *et al.* experimentally observed a transition range of 4.3 nm for pure PbS/TiO_2 in organic solvents.[29] As the electron affinity of the TiO_2 nanoparticles in organic solvent is 3.9 eV, and the electron affinity when dried is 4.45 eV (in our case, we assume the electron affinity of the TiO_2 film to be around −4.2 eV),[14] the critical diameter of 5.2 nm is quite reasonable due to the shift of the conduction band of TiO_2 film.

The accurate determination of the threshold size for electron injection is very important, because it determines the maximum absorption wavelength that can be usefully absorbed by the QDs to generate photoinjected charges in the operating device. The threshold size we found for thin shells (critical diameter 4.8 nm for 0.3 nm shell thickness) is even better than the reported value for PbS on TiO_2 in previous studies (~4.3 nm),[29] clearly indicating that the presence of the shell does not significantly affect the photoinduced electron transfer. The increased critical size for injection in our work, compared to ref. 29, could be ascribed to the shorted bifunctional linker (MAA) we applied, with

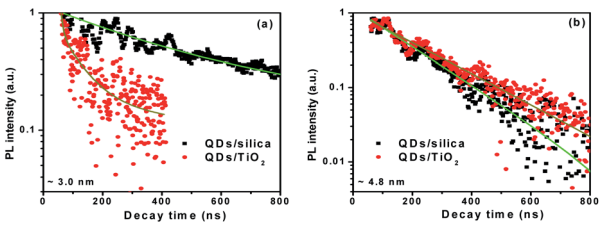

Fig. 4 Fluorescence decays of PbS@CdS QDs grafted on silica and TiO_2 for different PbS core diameter: (a) 3.0 nm and (b) 4.8 nm. The shell thickness is 0.2–0.3 nm. The excitation wavelength is λ_{ex} = 444 nm. All measurements were carried out at ambient temperature. The complete inhibition of charge injection in QD system with 4.8 nm core size is clearly visible, which reflects in almost similar PL decay time for TiO_2 and silica scaffold.

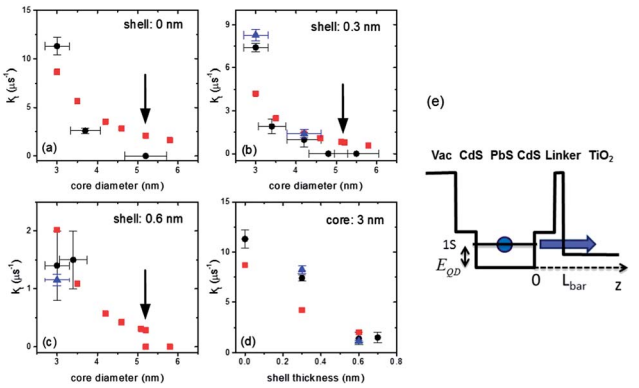

Fig. 5 Tunneling rate k_t as a function of core diameter for three different shell thickness: (a) 0 nm; (b) 0.3 nm; (c) 0.6 nm. (d) Tunneling rate k_t as a function of shell thickness for a fixed core size of 3.0 nm. Black circles: TiO_2, experiment; red squares: TiO_2, theory; blue triangles: SnO_2, experiment. (e) The band diagram of the QD and the tunneling process calculated in the text. Arrows in (a)–(c) indicate the limiting diameters of QD, at which the tunneling stops.

respect to 3-mercaptopropionic acid (MPA), since the shorter distance between the QD and the oxide increases the probability for electron tunnelling.

3.5 Electron transfer: the effect of shell thickness

To study the effect of shell thickness on electron transfer rate, we synthesized PbS@CdS QDs with different shell thickness and same core size.

As shown in Fig. S4a,† the first exciton peak of core@shell QDs exhibits a large blue shift compared to the starting PbS QDs, indicating a decrease of PbS core size during the cation exchange reaction. The first exciton absorption peak position for all the samples occurs at around ~900 nm, corresponding to a PbS core size of ~3.0 nm for all the considered PbS@CdS samples (Fig. S5†).[20] The average CdS shell thickness was varied from 0.2 to 0.6 nm, estimated by subtracting the core size evaluated from the position of the first excitonic peak from the overall QD size from TEM observations. The PL peak position also shows a red-shift after grafting QDs to SiO_2 or TiO_2 nanoparticles (Fig. S4b†), similarly to the previous discussion.

Fig. 6 displays the PL decay for a 3.0 nm core QD at different shell thickness. With respect to shell-free PbS QDs, PL in core@shell QDs exhibits much slower decay for both SnO_2 and TiO_2 (see also Fig. 5d).

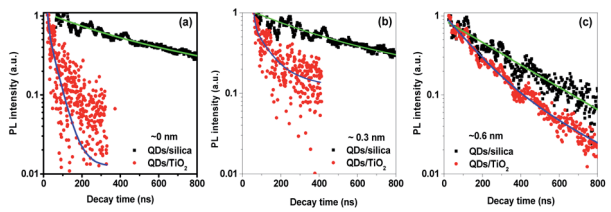

Fig. 6 Fluorescence decay spectra (λ_{ex} = 444) of PbS@CdS, PbS@CdS–TiO_2 with core size of 3.0 nm and shell thickness of 0, 0.3 and 0.6 nm. The spectrum of the PbS@CdS–SiO_2 system is reported as a benchmark.

Fig. 5d reports k_t as a function of shell thickness for a core size of 3.0 nm. The experimental results indicate that the presence of the shell contributes to inhibit exciton dissociation and charge injection at the QD–oxide interface. As expected, injection is faster in SnO_2 than in TiO_2 due to favorable band alignment (see Scheme 1). This effect on the electron transfer rate reflects the reduced probability of electrons leaking to the surface in thicker shell QDs, as predicted by the theoretical calculations (see below), since the presence of the shell inhibits the partial leakage of the electronic wave function into the outer part of the QD. However our results highlight that proper choice of a thin shell contributes to largely enhance QD stability and still allows efficient charge injection to take place.

3.6 Theoretical modeling

We applied the semi-classical approximation to estimate the escape time for an electron from the 1S-state of QD (see Fig. 5e). We first compute the quantum states of an isolated QD and find the position for the 1S state, which is separated from the QD bottom by the energy ΔE_{QD} (Fig. 5e). This energy gives a characteristic velocity of an electron in a QD. Then, the tunneling rate can be estimated as

$$K_t = A f_{QD} P_{tun}, \quad (3)$$

where $f_{QD} = v_e/2d_{QD}$ is a quasi-classical frequency of oscillation of electron in a QD, $v_e = \sqrt{\frac{2E_{QD}}{m_{eff}}}$ is the characteristic electron velocity in the 1S state and d_{QD} is the QD diameter.

The coefficient A is an empirical constant that takes into account a small fraction of the surface area of QD where the tunnel process takes place. The key parameter is the quasi-classical probability of tunneling:

$$P_{tun} = e^{-\frac{2}{\hbar}\int_0^{L_{bar}} dz|p(z)|}, p(z) = \sqrt{2m_{eff}(z)(E_{1S} - U(z))}, \quad (4)$$

where the integral is taken over the tunnel path going through the barrier, $U(z)$ is the electron potential along the tunneling path (Fig. 5e) and $m_{eff}(z)$ is the effective mass of the electron taken again along the tunneling path.

For the effective mass, we took: $0.09m_0$ for PbS and $0.2m_0$ for CdS, and m_0 for the linker and vacuum regions. The potential offsets in Fig. 5e are given by the affinity of the materials: −3.7 eV (CdS), −4.5 eV (PbS), and −4.2 eV (TiO_2). The tunnel constant $A = 7.23 \times 10^{-3}$ was chosen so as to match the experiment semi-quantitatively. This simple model reproduces the main trends observed in our experiments (see in Fig. 5 the comparison between theoretical calculations and experimental results). (1) The tunnel rate rapidly decreases with increasing core radius mainly because of the downshift of the 1S-state and the tunnel probability P_{tun} decreases exponentially. (2) As expected, tunneling weakens when increasing the shell thickness. This model does not take into account the density of states in the contact (TiO_2 or SnO_2) and is only valid when the kinetic energy of injected carriers is not too small. As the QD diameter increases, the tunneling rate approaches zero when the 1S-state energy becomes equal to the energy of the conduction band of

TiO_2. The limiting diameters of QD, at which the tunneling stops, are shown by arrows in Fig. 5. Our theory does not reproduce this behavior, yet it describes the trends for the QD diameters when tunneling is active.

4. Conclusions and perspectives

In summary, we investigated the photoinduced electron transfer between PbS@CdS core@shell QDs and different types of metal oxide semiconducting mesoporous films. We demonstrated the modulation of the charge transfer rate from QD to oxide by varying QD size, shell thickness and type of oxide. As expected from the electronic band alignment, the charge transfer is highly favored in smaller sized QDs with very thin shell and is maximized in SnO_2 due to its lower electron affinity compared to TiO_2. Modeling of the escape time for an electron from the 1S-state of QD to the oxide using the semi-classical approximation is in good agreement with experiments, and provides us with a robust description of the processes taking place in this system. We demonstrated that such core@shell structures, exhibiting much higher stability than traditional uncoated PbS QDs, still preserve ability to transfer photogenerated charges from their excited state to a wide bandgap semiconductor.

In particular, we demonstrated that the threshold size for electron transfer for pure PbS QD is 5.2 ± 0.3 nm. The threshold size reduces to 4.8 ± 0.3 nm in a core@shell system with 0.3 nm thick shell. This observation is crucial for the exploitation of these QDs in third generation solar cells. The decrease in threshold size from 5.2 nm to 4.8 nm results in a shift of the first excitonic peak absorbance from ~1450 nm to ~1300 nm, indicating that this core@shell system is still active in the NIR region. At the expense of negligible reduction of spectral band absorbance, the core@shell system composed of PbS core and CdS shell with suitable core size and shell thickness is still able to inject photoexcited electrons to TiO_2 and SnO_2 nanoparticles and can be fruitfully applied to overcome one of the major challenges in QD solar cells, related to mid- and long-term stability of QDs.

Author contributions

The manuscript was written through contributions (conceptual, experimental, theoretical) of all authors. All authors have given approval to the final version of the manuscript.

Conflict of interest

The authors declare no competing financial interests.

Acknowledgements

A.V. acknowledges the European Commission for partial funding under the contract F-Light Marie Curie no. 299490. The authors acknowledge the European Commission for partial funding under the contract WIROX no. 295216. I.C. acknowledges Regione Lombardia under X-Nano Project ("Emettitori di elettroni a base di nano tubi di carbonio e nano strutture di ossidi metallici quasi monodimensionale per lo sviluppo di sorgenti a raggi X") for partial funding. G.S.S. acknowledges OIKOS s.r.l. for funding. M.M.N. acknowledges the Italian MIUR under the project FIRB RBAP114AMK "RINAME" for partial funding. H.L. acknowledges FRQNT for a PhD scholarship. F.R. acknowledges the Canada Research Chairs program for partial salary support. F.R. is grateful to the Alexander von Humboldt Foundation for a F.W. Bessel Award. F.R. and D.M. acknowledge NSERC for funding from Discovery, Équipe and Strategic grants and MDEIE for partial funding through the project WIROX. F.R. is supported by Elsevier through a grant from Applied Surface Science and H.Z. acknowledges funding from NSERC through PDF fellowship. I.C. and A.V. acknowledge Regione Lombardia for partial funding under the project "Tecnologie e materiali per l'utilizzo efficiente dell'energia solare".

Notes and references

1 G. Konstantatos, I. Howard, A. Fischer, S. Hoogland, J. Clifford, E. Klem, L. Levina and E. H. Sargent, *Nature*, 2006, **442**, 180–183.
2 L. Y. Chang, R. R. Lunt, P. R. Brown, V. Bulovic and M. G. Bawendi, *Nano Lett.*, 2013, **13**, 994–999.
3 Y. Shirasaki, G. J. Supran, M. G. Bawendi and V. Bulovic, *Nat. Photonics*, 2013, **7**, 13–23.
4 K.-S. Cho, E. K. Lee, W.-J. Joo, E. Jang, T.-H. Kim, S. J. Lee, S.-J. Kwon, J. Y. Han, B.-K. Kim, B. L. Choi and J. M. Kim, *Nat. Photonics*, 2009, **3**, 341–345.
5 M. A. Green, *Phys. E*, 2002, **14**, 65–70.
6 A. J. Nozik, *Phys. E*, 2002, **14**, 115–120.
7 A. H. Ip, S. M. Thon, S. Hoogland, O. Voznyy, D. Zhitomirsky, R. Debnath, L. Levina, L. R. Rollny, G. H. Carey, A. Fischer, K. W. Kemp, I. J. Kramer, Z. Ning, A. J. Labelle, K. W. Chou, A. Amassian and E. H. Sargent, *Nat. Nanotechnol.*, 2012, **7**, 577–582.
8 J. Tang, K. W. Kemp, S. Hoogland, K. S. Jeong, H. Liu, L. Levina, M. Furukawa, X. H. Wang, R. Debnath, D. K. Cha, K. W. Chou, A. Fischer, A. Amassian, J. B. Asbury and E. H. Sargent, *Nat. Mater.*, 2011, **10**, 765–771.
9 B. O. Dabbousi, J. RodriguezViejo, F. V. Mikulec, J. R. Heine, H. Mattoussi, R. Ober, K. F. Jensen and M. G. Bawendi, *J. Phys. Chem. B*, 1997, **101**, 9463–9475.
10 L. Dworak, V. V. Matylitsky, V. V. Breus, M. Braun, T. Basche and J. Wachtveitl, *J. Phys. Chem. C*, 2011, **115**, 3949–3955.
11 L. Etgar, D. Yanover, R. K. Capek, R. Vaxenburg, Z. S. Xue, B. Liu, M. K. Nazeeruddin, E. Lifshitz and M. Gratzel, *Adv. Funct. Mater.*, 2013, **23**, 2736–2741.
12 Z. J. Ning, H. N. Tian, C. Z. Yuan, Y. Fu, H. Y. Qin, L. C. Sun and H. Agren, *Chem. Commun.*, 2011, **47**, 1536–1538.
13 S. Ruhle, M. Shalom and A. Zaban, *ChemPhysChem*, 2010, **11**, 2290–2304.
14 M. Danek, K. F. Jensen, C. B. Murray and M. G. Bawendi, *Chem. Mater.*, 1996, **8**, 173–180.
15 S. A. Ivanov, A. Piryatinski, J. Nanda, S. Tretiak, K. R. Zavadil, W. O. Wallace, D. Werder and V. I. Klimov, *J. Am. Chem. Soc.*, 2007, **129**, 11708–11719.

16 S. Kim, B. Fisher, H. J. Eisler and M. Bawendi, *J. Am. Chem. Soc.*, 2003, **125**, 11466–11467.
17 B. De Geyter, Y. Justo, I. Moreels, K. Lambert, P. F. Smet, D. Van Thourhout, A. J. Houtepen, D. Grodzinska, C. D. Donega, A. Meijerink, D. Vanmaekelbergh and Z. Hens, *ACS Nano*, 2011, **5**, 58–66.
18 J. M. Pietryga, D. J. Werder, D. J. Williams, J. L. Casson, R. D. Schaller, V. I. Klimov and J. A. Hollingsworth, *J. Am. Chem. Soc.*, 2008, **130**, 4879–4885.
19 E. Ryu, S. Kim, E. Jang, S. Jun, H. Jang, B. Kim and S. W. Kim, *Chem. Mater.*, 2009, **21**, 573–575.
20 H. G. Zhao, M. Chaker, N. Q. Wu and D. L. Ma, *J. Mater. Chem.*, 2011, **21**, 8898–8904.
21 H. G. Zhao, D. F. Wang, T. Zhang, M. Chaker and D. L. Ma, *Chem. Commun.*, 2010, **46**, 5301–5303.
22 H. G. Zhao, H. Y. Liang, B. A. Gonfa, M. Chaker, T. Ozaki, P. Tijssen, F. Vidal and D. Ma, *Nanoscale*, 2014, **6**, 215–225.
23 B. R. Hyun, A. C. Bartnik, L. F. Sun, T. Hanrath and F. W. Wise, *Nano Lett.*, 2011, **11**, 2126–2132.
24 B. A. Gonfa, H. Zhao, J. Li, J. Qiu, M. Saidani, S. Zhang, R. Izquierdo, N. Wu, M. A. El Khakani and D. Ma, *Sol. Energy Mater. Sol. Cells*, 2014, **124**, 67–74.
25 T. Zhang, H. G. Zhao, D. Riabinina, M. Chaker and D. L. Ma, *J. Phys. Chem. C*, 2010, **114**, 10153–10159.
26 W. Stober, A. Fink and E. Bohn, *J. Colloid Interface Sci.*, 1968, **26**, 62–69.
27 A. Braga, S. Giménez, I. Concina, A. Vomiero and I. n. Mora-Seró, *J. Phys. Chem. Lett.*, 2011, **2**, 454–460.
28 D. R. Pernik, K. Tvrdy, J. G. Radich and P. V. Kamat, *J. Phys. Chem. C*, 2011, **115**, 13511–13519.
29 B. R. Hyun, Y. W. Zhong, A. C. Bartnik, L. F. Sun, H. D. Abruna, F. W. Wise, J. D. Goodreau, J. R. Matthews, T. M. Leslie and N. F. Borrelli, *ACS Nano*, 2008, **2**, 2206–2212.
30 H. C. Leventis, F. O'Mahony, J. Akhtar, M. Afzaal, P. O'Brien and S. A. Haque, *J. Am. Chem. Soc.*, 2010, **132**, 2743–2750.
31 S. W. Clark, J. M. Harbold and F. W. Wise, *J. Phys. Chem. C*, 2007, **111**, 7302–7305.
32 D. F. Wang, H. G. Zhao, N. Q. Wu, M. A. El Khakani and D. L. Ma, *J. Phys. Chem. Lett.*, 2010, **1**, 1030–1035.
33 M. Gratzel, *Nature*, 2001, **414**, 338–344.
34 K. Tvrdy, P. A. Frantsuzov and P. V. Kamat, *Proc. Natl. Acad. Sci. U. S. A.*, 2011, **108**, 29–34.
35 K. R. Gopidas, M. Bohorquez and P. V. Kamat, *J. Phys. Chem.*, 1990, **94**, 6435–6440.